Effect of channel-confinement and aiding/opposing buoyancy on the two-dimensional laminar flow and heat transfer across a square cylinder

Atul Sharma [a,*], V. Eswaran [b]

[a] *Department of Mechanical Engineering, Indian Institute of Technology Bombay, Mumbai 400 076, India*
[b] *Department of Mechanical Engineering, Indian Institute of Technology, Kanpur, 208 016 UP, India*

Abstract

The effect of channel-confinement of various degree (blockage ratio of 10%, 30% and 50%) on the upward flow and heat transfer characteristics around a heated/cooled square cylinder is studied by considering the effect of aiding/opposing buoyancy at $-1 \leqslant Ri \leqslant 1$, for $Re = 100$ and $Pr = 0.7$. With increasing blockage ratio, the minimum heating (critical Ri) required for the suppression of vortex shedding decreases up to a certain blockage ratio ($=30\%$), but thereafter increases. The influence of buoyancy and channel-confinement on the recirculation length, drag and lift coefficient, pumping power, Strouhal number and heat transfer from the cylinder, is also investigated.
© 2005 Elsevier Ltd. All rights reserved.

Keywords: Square cylinder; Channel; Blockage ratio; Buoyancy; Vortex shedding; Heat transfer

1. Introduction

Heat and fluid flow are generally either external (unconfined) or internal (confined). Some problems have several of the characteristics of both unconfined and confined flows. An example of such a case is the flow across a cylinder located on the centerline of a two-dimensional channel with fixed walls which will be referred to here as channel-confined flow. The confined flow configuration is a natural one for heating and cooling fluids in many engineering applications. The flow and heat transfer characteristics are strongly influenced by the buoyancy force when the flow velocity is not very high and the temperature difference between the body surface and ambient fluid is large. The free and forced convection effects are comparable under such situations. The vortex shedding also becomes more complicated. Most previous investigations of combined flow and heat transfer in such situations have focussed on circular cylinders. However, flow around the square cylinder is also an important fundamental problem of engineering interest and is investigated here.

In comparison with the unconfined flow case, two new parameters have to be taken into account for an upward channel-confined flow case, i.e., the inflow profile and the blockage ratio ($\equiv B/L$, where B is the width of the cylinder and L is distance between the channel walls). Most of the previous heat transfer studies on channel-confined flow across a square cylinder was done

---

* Corresponding author. Tel.: +91 22 25767505; fax: +91 22 25726875.
E-mail address: atuls@me.iitb.ac.in (A. Sharma).

Nomenclature

B	width of the square cylinder
c_p	specific heat of the fluid
C_D^{CC}	total drag coefficient for the channel-confined flow, Eq. (1)
C_{Dcyl}	cylinder drag coefficient, Eq. (2)
C_{Dch}	channel drag coefficient, Eq. (2)
C_L	lift coefficient $[= F_L / \frac{1}{2}\rho v_\infty^2 B]$
f	frequency of vortex shedding
F_L	lift force on the cylinder
Gr	Grashof number $[= g\beta(T_W - T_\infty)B^3/v^2]$
H	height of the computational domain and the channel
H_D	non-dimensional distance between top surface of cylinder and exit plane
H_U	non-dimensional distance between inlet plane and bottom surface of cylinder
L	distance between the channel walls
L_r	non-dimensional recirculation length
n	cylinder surface normal direction
Nu	average Nusselt number $[= \partial\theta/\partial n]$
p	pressure
P	non-dimensional pressure $[= p/\rho v_\infty^2]$
Pr	Prandtl number $[= \mu c_p/k]$
Re	Reynolds number $[= v_\infty B/v]$
Ri	Richardson number $[= Gr/Re^2]$
St	Strouhal number $[= fB/v_\infty]$
T	temperature
T_∞	free-stream or inlet temperature
u	cross-stream velocity
v_∞	free-stream velocity and the mean-channel inlet velocity
v	stream-wise velocity

$\dot{w}$	pumping power, Eq. (4)
X	non-dimensional cross-stream dimension of coordinates $[= x/B]$
Y	non-dimensional stream-wise dimension of coordinates $[= y/B]$

Greek symbols

δ	size of the clustered CV
Φ	pumping power coefficient, Eq. (3)
v	Kinematic viscosity of the fluid
θ	non-dimensional temperature $[= (T - T_\infty)/(T_W - T_\infty)]$
τ	non-dimensional time $[= t/(B/v_\infty)]$

Subscripts

b	bottom face of the cylinder
c	cylinder average
cl	lower critical value
cu	upper critical value
l	left face of the cylinder
r	right face of the cylinder
rms	root mean square
t	top face of the cylinder
W	surface of the cylinder

Superscripts

CC	channel-confined
FC	forced convection
MC	mixed convection
UC	unconfined

for the forced convection case [1–5]. In our earlier study [5], a detailed examination of the effect of channel-confinement on the flow structure and heat transfer from the cylinder at various Reynolds number was done for both constant uniform heat flux and constant cylinder temperature boundary conditions. With increasing blockage ratio, the Reynolds number for the onset of vortex shedding was found to increase and then decrease. An increase in Strouhal number, drag coefficient, pumping power and cylinder Nusselt number was also observed with increasing blockage ratio.

For the mixed-convection case, the buoyancy parameter $Ri \equiv Gr/Re^2$, which is known as the Richardson number, provides a measure of the influence of free convection in comparison with the forced convection. Chang and Sa [6] did a detailed numerical study of the effect of buoyancy on the flow past a hot/cold circular cylinder, at $Re = 100$ for $-1 \leqslant Ri \leqslant 1$ and found sup-

pression of vortex shedding at a critical Ri of 0.15. The critical Richardson number found by different researchers for free-stream flow across a circular cylinder have been compared in our earlier study [7]. The suppression of vortex shedding into steady twin vortices, previously observed experimentally for the circular cylinder, was also found [7] for the more bluff square cylinder beyond a certain heating ($Ri = 0.15$) of the cylinder for $Re = 100$ and $Pr = 0.7$.

Most of the study on the effect of channel-confinement and buoyancy on flow across a cylinder have been done for the circular cylinder [8–11]. Farouk and Güceri [8] initiated the numerical simulation of the effect of aiding buoyancy on flow across a circular cylinder maintained at constant temperature within adiabatic channel walls but restricted their study to steady flows. Ho et al. [9] also studied the aiding buoyancy in the steady flow regime with uniform inlet velocity profile for both

unconfined and channel-confined (adiabatic channel-wall) upward flow across a circular cylinder at $Re = 20$, 40 and 60, $0 \leqslant Ri \leqslant 4$, and blockage ratio of 50%, 25%, 16.67% and 0%. They developed a forced and a mixed convection heat transfer correlation for the steady flow.

Nakabe et al. [10] studied the effect of buoyancy on the channel-confined (channel walls maintained at ambient temperature) flow across a heated or a cooled circular cylinder with parabolic inlet velocity profile, by a finite difference method. Three cases of the flow configurations were calculated: (1) aiding buoyancy at $Re = 80$ and 120, $0 \leqslant Ri \leqslant 1.6$ and blockage ratios of 30% and 15%, (2) opposing buoyancy at $Re = 50$, $-1 \leqslant Ri \leqslant 0$ and a blockage ratio of 15%, and (3) cross-stream buoyancy at $Re = 80$ and a blockage ratio of 30%. For the aiding buoyancy case, the authors found three main results: first, at constant Re, the value of Ri at which the vortex shedding degenerates (into twin vortices) decreases with increasing blockage ratio; second, at constant blockage ratio, the value of Ri at which vortex shedding degenerates increases with Re; and third, at constant Ri, the value of Re at which vortex shedding starts goes on increasing with the increasing blockage ratio.

Singh et al. [11] numerically studied steady and unsteady periodic mixed convection heat transfer for flow of air around a hot/cold circular cylinder in a vertical adiabatic channel, with parabolic inlet velocity profile at $Re = 100$, $-1 < Ri < 1$ and a blockage ratio of 25%. They found the "breakdown" of Karman vortex street at $Ri = 0.15$. All the work discussed above on the channel-confined mixed-convective flow are for the circular cylinder. Virtually no analogous results have been found for the square cylinder other then those of Biswas et al. [12] who numerically investigated the effect of cross-stream buoyancy on the channel-confined flow.

The present work is continuation of our previous work [5,7,13]. The objective of this investigation is to study the effect of aiding and opposing buoyancy, as well as the effect of the proximity of the adiabatic bounding (channel) walls on the flow and heat transfer characteristics across a heated/cooled square cylinder for various Reynolds number, Richardson number and blockage ratios. The study attempts to understand how the channel-confinement of various degree at a constant Re and increasing Re at a constant blockage ratio effects the buoyancy induced breakdown of Kármán vortex street for the square cylinder. For a Reynolds number ($=50$) where there are normally steady twin vortices in the wake of the cylinder for the channel-confinement case ($B/H = 30\%$), we investigate whether vortex shedding is triggered after a certain minimum cooling of the cylinder. Furthermore, the objective is to generate a numerical database for the flow and heat transfer parameters with respect to Richardson number and blockage ratio for $Re = 100$.

2. Physical description of the problem, governing equations and boundary conditions

The geometry and the relevant dimensions considered for analysis are schematically shown in Fig. 1. A fixed two-dimensional square cylinder with side B (which is also the non-dimensionalising length scale) heated or cooled to a constant temperature T_W is exposed to a constant free-stream upward velocity v_∞ and temperature T_∞, as shown in Fig. 1(a). In order to make the problem computationally feasible, artificial confining boundaries are placed around the flow where "free-slip" boundary conditions are used. The channel-confined flow case is obtained when "no-slip" boundary conditions are applied to the two adiabatic channel walls of finite length placed vertically at a distance of $L/2$ on either side of the center of the cylinder, as shown in Fig. 1(b). We assume that the fluid enters the channel under fully developed conditions, i.e., a parabolic velocity profile (with the average velocity, $v_{av} = v_\infty$) and temperature T_∞. The results in this case is also applicable for the channel of infinite length with a constant v_∞ inlet velocity profile, as this flow will be fully developed before it reaches the cylinder. This allows us to compare the confined flow cases with the unconfined flow cases (where the inlet velocity profile is constant). The various degree of confinement (B/L) is obtained by varying the distance L between the channel walls.

A preliminary study was done to fix the position of artificial confining boundaries (for the free-stream flow), inlet and outlet boundary relative to the cylinder denoted by L, H_U and H_D, respectively (Fig. 1). It was found [5,7,13] that there is negligible change in the results with further increase in $L = 30$, $H_U = 5$ and
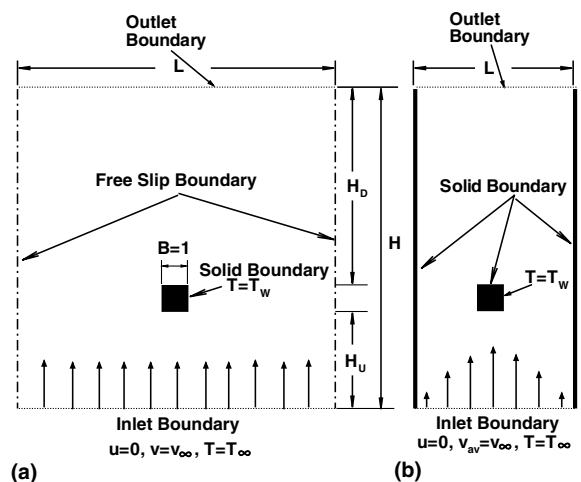

Fig. 1. Computational domain for (a) unconfined and (b) channel-confined vertical-flow problem and the associated parameters.

$H_D = 34$ for the unconfined flow; and $H_U = 8.5$ and $H_D = 16.5$ for the channel-confined flow.

The unsteady, conservative, and dimensionless form of the Navier–Stokes equations [7] in two dimensions for the incompressible flow of a constant viscosity fluid is numerically solved in the present study. In these equations, the velocity is non-dimensionalised with v_∞ (which is the constant inlet velocity for the unconfined flow and is the mean-channel inlet velocity for the channel-confined flow case), the spatial coordinates with cylinder width B and the pressure by ρu_∞^2. The dimensionless temperature variable is given by $\theta \equiv (T - T_\infty)/(T_W - T_\infty)$. The Reynolds number, Prandtl number and Richardson number are the governing flow parameter for this problem. The boundary conditions are discussed in our earlier work [5,7].

3. Numerical details

The non-uniform grid structure, with a grid of size $\delta = 0.01$ clustered around the cylinder over a distance of 1.5 units, and the grid independence results for the unconfined case was discussed in our earlier investigation [7]. For the confined flow case, the grid structure is similar in the X-direction and the details can be found elsewhere [5]. Uniform clustered grid size of δ has been used over the entire height of the channel (in the Y-direction) for a blockage ratio of 30%, 40%, and 50% to adequately capture increased cylinder-channel wall interaction resulting in a grid size of 323×334, 323×250 and 323×200, respectively. Grid independence tests were accomplished satisfactorily [14] for the channel-confined flow using four grid sizes (169×48, 222×96, 323×200 and 363×240) at the largest blockage ratio of 50% and $Ri = -1$. It is found that the rms value of lift coefficient, as compared to the other parameters, has the greatest sensitivity to the number of grid points in the domain and its value has a maximum difference of 12% and 3% on the first two grid sizes when compared to the finest grid size. The percentage change of this quantity between the final two grid sizes is 0.26%. The time step was set at 8×10^{-4}, since a smaller time step had no significant influence on the results. The impulsive flow initial condition has been used.

A solution methodology (Semi-Explicit method) using finite volume method on a non-staggered non-orthogonal grid, applicable to complex geometries, has been developed by Eswaran and Prakash [15]. However, the code has been substantially modified here to remove some of the features required only for non-orthogonal grids and was made strictly two-dimensional, to avoid excessive computation for the two-dimensional orthogonal geometry problem attempted here. Furthermore, the third-order upwind QUICK convection scheme has been consistently implemented in the code. The details of the

method have been presented by Sharma and Eswaran [16].

4. Results and discussion

In this study, the following range of parameters are considered: blockage ratio, $B/L = 0\%$, 10%, 30% and 50%, and Richardson number, $Ri = \pm 0.25$, ± 0.5, ± 0.75 and ± 1 (positive values for the aiding and negative values for the opposing buoyancy case) for Reynolds number, $Re = 100$, and Prandtl number, $Pr = 0.7$ (as for air). The unconfined flow case corresponds to $B/L = 0\%$ although free-slip confining wall with a blockage ratio of 3.34% is used here to make the problem computationally feasible. Other Richardson numbers have been investigated for the aiding buoyancy case to determine the critical Ri for the breakdown of Kármán vortex street, at various blockage ratios. Furthermore, $Re = 50$ and 150 have been investigated for $B/L = 30\%$.

The accuracy of the simulation is validated in our earlier work [5] for the Strouhal number and Drag coefficient dependence on Reynolds number for various blockage ratio at $Ri = 0$.

4.1. Flow and isotherms pattern

Figs. 2–4 shows the vorticity contours for $B/L = 10\%$, 30% and 50%, respectively, under the influence of aiding and opposing buoyancy at $Re = 100$. The vorticity contours show a wavering motion which increases with increased cooling (decreasing $Ri < 0$) of the cylinder and decreases with increased heating(increasing $Ri > 0$) before it ceases at $Ri = 0.4$, 0.25 and 0.5 for $B/L = 10\%$, 30% and 50%, respectively [shown in Figs. 2(f), 3(f) and 4(f)]. Ri_{cl} corresponds to the upper limit of the unsteady periodic flow whereas Ri_{cu} to the breakdown of Kármán vortex street. Thus, the breakdown of Kármán vortex street occurs between a lower and upper value of critical Richardson number, $Ri_{cl} = 0.35$, 0.2 and 0.45 and $Ri_{cu} = 0.4$, 0.25 and 0.5 for $B/L = 10\%$, 30% and 50%, respectively. These results for the square cylinder on the effect of buoyancy are in accordance with the physics that are well known in the circular cylinder wake [6] in an unconfined flow. Chang and Sa [6] discussed that the strength of the shear layer increases and the roll-up process is more activated with increased cooling of the circular cylinder because the velocity in the wake region is reduced by the negative buoyancy force of the cold air. They also mentioned that heating imparts stability to the vortex street with an increase in the velocity in the wake region. With increased channel spacing from $B/L = 10\%$ to 30%, the channel-wall tries to confine the streamlines near to the cylinder and an increase in the velocity of the fluid in the wake
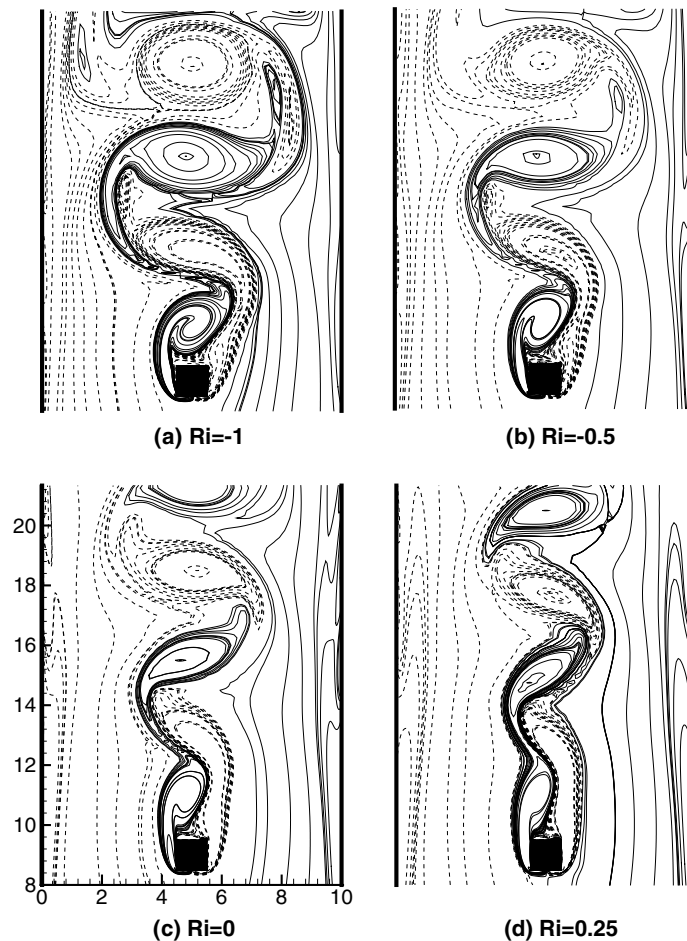
Fig. 2. Instantaneous vorticity contours for different Ri, under the influence of aiding and opposing buoyancy, at a blockage ratio of 10% and $Re = 100$. Note that the solid and dashed lines represent the positive and negative vorticity, respectively.

region imparts channel-wall induced stability to the vortex street and thus less heating is required to stabilize the flow. However, with further increase in blockage ratio, the velocity of the fluid emanating from between the side faces of the cylinder and the channel wall increases. This flow jets outward sending particles into the wake cavity and thus, more heating is required to diminish the entrainment till it eventually vanish for the breakdown of Kármán vortex street at $B/L = 50\%$. The results on the decrease in the stability of the flow when the blockage ratio increases from 30% to 50% has not been reported before for both circular and square cylinders.

For the unsteady cases, Fig. 2 show an almost symmetric distribution (about the channel centerline) of the vorticity generated at the channel walls. However, this symmetry is lost for $B/L = 30\%$ and 50%, shown in Figs. 3 and 4. Thus, for a heated/cooled cylinder at the blockage ratio of 10%, the time-dependent flow motion is only noticeable near the cylinder and the flow in

the region near to the channel wall is close to the one observed for the steady flow regime. However, as the blockage ratio increases to $B/L \geqslant 30\%$, the near wall (channel) flow also becomes unsteady.

The instantaneous isotherms (figures not included) for the same cases showed that the roll-up or wavering motion of the isotherms increases with increased cooling of the cylinder and decreases with increased heating of the cylinder before it ceases at certain Ri. Furthermore, the roll-up decreases with increasing blockage ratio at a constant Ri. Thus, the isotherms plots have a close resemblance with the vorticity contours shown in Figs. 2–4, indicating that the energy convected away from the cylinder surface is bound tightly inside the vortices.

4.2. Flow parameters

The time-averaged flow field in a periodic flow (except at $Ri = -0.75$ and -1 for $B/L = 0\%$) is similar to
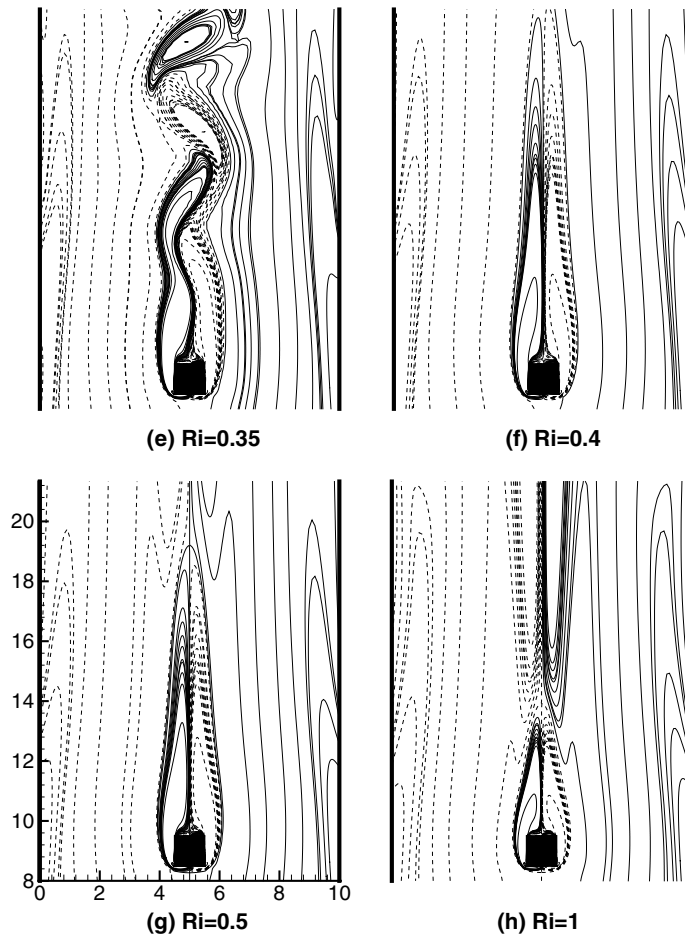
Fig. 2 (*continued*)

steady flow with a twin-vortex recirculating region. The recirculation length is defined as stream-wise distance from the top surface of the cylinder to the re-attachment point along the wake centerline. With increased cooling (decreasing $Ri < 0$), Fig. 5(a) shows that the mean recirculation length decreases at $B/L = 0$ and 10% in contrast to its increasing trend at $B/L = 30\%$ and 50%. The alternate generation of vortex on the wall of the cylinder and its shedding is due to the periodic variation of pressure acting on the side faces of the cylinder. With increased cooling at $B/L = 10\%$, the roll-up of the vorticity (generated on the side faces of the cylinder) on the top surface of the cylinder increases (Fig. 2(a)–(c)) which results in the decrease in the mean recirculation length. Further increase in the blockage ratio ($B/L \geqslant 30\%$) suppresses the roll-up with a reduced entrainment of the far away fluid into the wake region due to stronger interaction between the channel boundary layer and the cylinder shear layer, shown more prominently for $Ri = -1$ in Figs. 2–4 and thus, increases the mean recirculation length with increased cooling. However, with increased heating the recirculation length increases monotonically in the periodic flow regime, in contrast to its decreasing trend in the steady flow regime, shown in the figure by open and filled symbols, respectively. Furthermore, with increasing Ri in the periodic flow regime, the figure show a local minimum at $Ri = 0$ for $B/L = 30\%$ and 50%. For fixed Ri, Fig. 5(b) show a local maximum for $Ri \leqslant 0.25$ and a local minimum for the steady flow cases at $Ri \geqslant 0.5$, both at $B/L = 30\%$.

For the aiding and opposing buoyancy cases, Fig. 6(a) shows that the Strouhal number increases monotonically with increasing Ri at a constant blockage ratio before it suddenly becomes zero due to the breakdown of the Kármán vortex street. The figure also shows that the Strouhal number increases monotonically with increasing blockage ratio due to the acceleration of the cylinder-wall boundary layer.

The drag force acting on the square cylinder includes pressure drag F_{Dp} and viscous drag F_{Dv}, which

(a) Ri=-1 **(b) Ri=-0.5** **(c) Ri=-0.25** **(d) Ri=0**

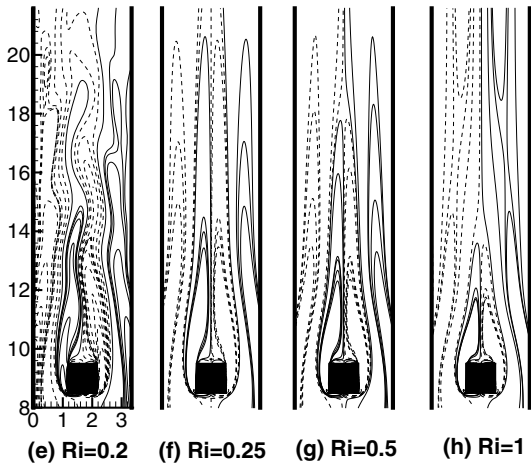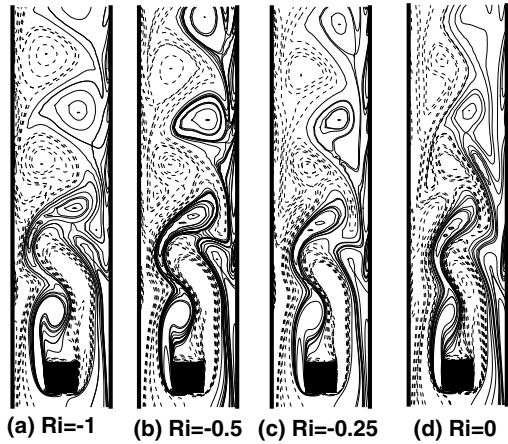**(e) Ri=0.2** **(f) Ri=0.25** **(g) Ri=0.5** **(h) Ri=1**

Fig. 3. Instantaneous vorticity contours for different Ri, under the influence of aiding and opposing buoyancy, at a blockage ratio of 30% and $Re = 100$. Note that the solid and dashed lines represent the positive and negative vorticity, respectively.
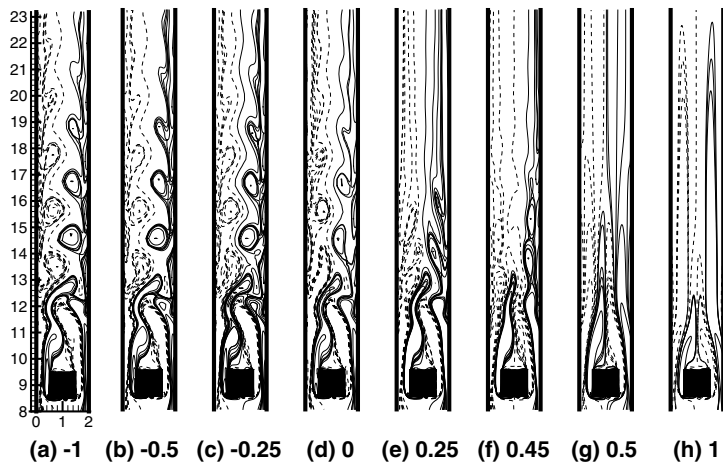
correspond to the power needed to pump the fluid through the cylinder. For the channel-confined flow, the total drag coefficient includes cylinder as well as channel drag coefficients:

$$C_D^{CC} = C_{Dcyl} + C_{Dch} \tag{1}$$

where

$$C_{Dcyl} = 2 \int_0^1 P dX + \frac{2}{Re} \int_0^1 \frac{\partial V}{\partial X} dY \quad \text{and}$$

$$C_{Dch} = 2 \times \frac{2}{Re} \int_0^{H/B} \frac{\partial V}{\partial X} dY \tag{2}$$

and the non-dimensional pumping power coefficient [5] can be expressed as

$$\Phi = C_D^{CC} Re^2 \tag{3}$$

from which the pumping power (per unit length of the cylinder) is obtained by

$$\dot{w} = \Phi \times \frac{1}{2} \rho v^2 \times \frac{v_\infty}{B} \tag{4}$$

Fig. 6(b) shows the effect of buoyancy on the various drag coefficients at various blockage ratio for $H/B = 26$. We can draw the following conclusions: (1) At a constant Ri, the C_D^{CC} (and thus, the pumping power), C_{Dcyl}, and $C_{Dch} (\equiv C_D^{CC} - C_{Dcyl})$ increase with the blockage ratio; (2) at the same blockage ratio, the minimum C_{Dcyl} occurs at $Ri = 0$ for unconfined flow whereas for the channel-confined flow, it can be observed to occur for the largest value of Ri (Ri_{cl}) at which the vortex shedding occur (except at $B/L = 50\%$, where C_{Dcyl} does not change appreciably with increasing Ri); (3) the channel drag coefficient decreases with increased heating and increases with increased cooling; (4) the total drag coefficient/pumping power decreases monotonically with increasing Ri at $B/L = 30\%$ and 50%, is higher at

(a) -1 **(b) -0.5** **(c) -0.25** **(d) 0** **(e) 0.25** **(f) 0.45** **(g) 0.5** **(h) 1**

Fig. 4. Instantaneous vorticity contours for different Ri, under the influence of aiding and opposing buoyancy, at a blockage ratio of 50% and $Re = 100$. Note that the solid and dashed lines represent the positive and negative vorticity, respectively.
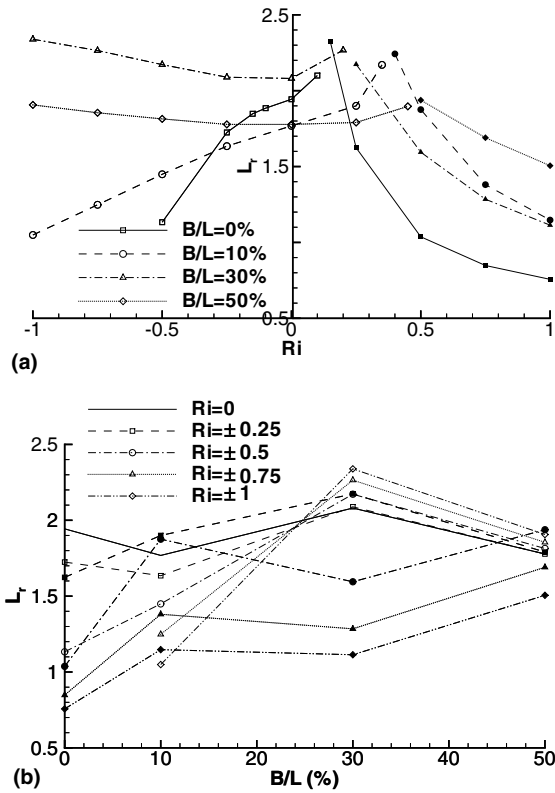
Fig. 5. Variation of non-dimensional recirculation length with (a) Richardson number and (b) blockage ratio at $Re = 100$. Note that filled and open symbols in (a) correspond to steady and unsteady-periodic flow and those in (b) to the aiding and opposing buoyancy cases, respectively.

$B/L = 10\%$ and lower at $B/L = 0\%$ for a cooled cylinder when compared with one heated by the same temperature difference.

Fig. 7(a) shows that the variation of rms value of lift coefficient decreases monotonically with increasing Ri

before it vanishes at certain Ri (for the aiding buoyancy). With increasing blockage ratio for the channel-confined flow, Fig. 7(b) shows a monotonic decrease in C_{Lrms} for the opposing buoyancy case whereas a local minimum can be seen at $B/L = 30\%$ for the aiding buoyancy cases at $Ri = 0$ and 0.25.

The vortex shedding is obtained by long time computations automatically initiated by computer round-off errors, thus eliminating the need to perturb the solution. Fig. 8 shows the temporal variation of lift coefficient and confirms that the degeneration of vortex shedding occurs between $Ri_{cl} = 0.35$, 0.2 and 0.45 and $Ri_{cu} = 0.4$, 0.25 and 0.5 at $B/L = 10\%$, 30% and 50%, respectively. Fig. 8(b), (d) and (f) also shows a monotonic decay in the amplitude of variation of lift coefficient in the zoomed view on the top-right corner whereas a monotonic rise can be seen for the vortex-shedding cases in the other figures.

4.3. Average Nusselt number

Fig. 9 compares the average Nusselt number for the cylinder and each of its faces versus blockage ratio at a constant Richardson number. The figure show a monotonic increase in the Nusselt number for the cylinder and its faces with increasing blockage ratio, except at the top face for $Ri \leqslant 0.25$. As compared to the unconfined flow, the top face Nusselt number is shown to be more for the channel-confined case at $B/L = 10\%$. With further increase in blockage ratio, three different trends of variation of top face Nusselt number can be observed in the figure. First, Fig. 9(a) and (b) show a monotonic decreasing trend for $Ri \leqslant -0.75$, second, Fig. 9(c)–(e) show a local minimum at $B/L = 30\%$, and third, Fig. 9(f)–(h) show an increasing trend in the steady flow regime for $Ri \geqslant 0.5$. With increasing Ri, the figure show a monotonic increase in the Nusselt number for the cylinder at a constant blockage ratio.
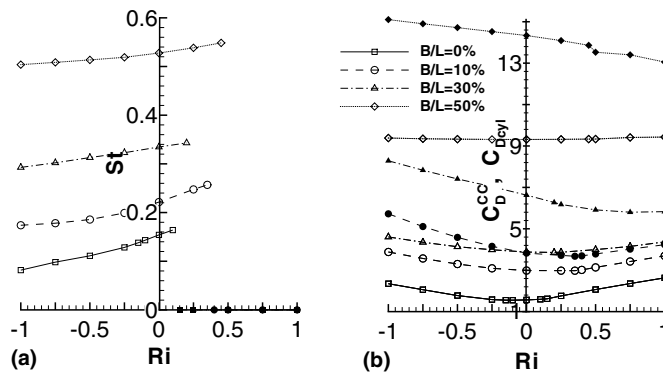

Fig. 6. Effect of buoyancy on (a) Strouhal number and (b) total and cylinder drag coefficient for various blockage ratios at $Re = 100$. Note that filled and unfilled symbols in (b) represent C_D^{CC} and C_{Dcyl}, respectively; and $C_D^{CC} - C_{Dcyl}$ represents the channel drag coefficient.
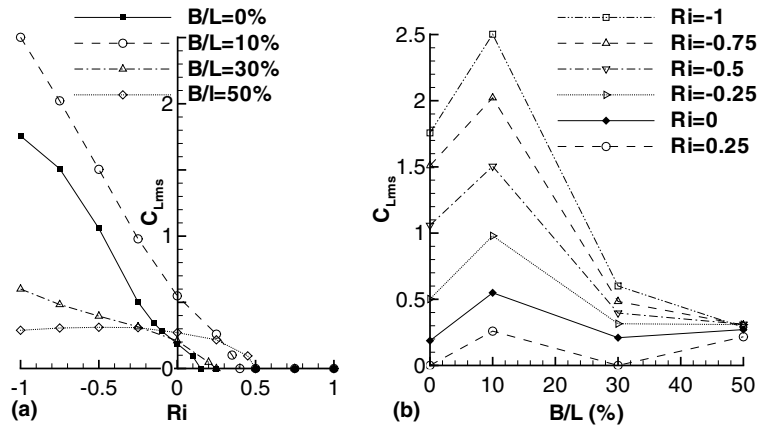
Fig. 7. Variation of rms value of lift coefficient with (a) Richardson number and (b) blockage ratio, at $Re = 100$.
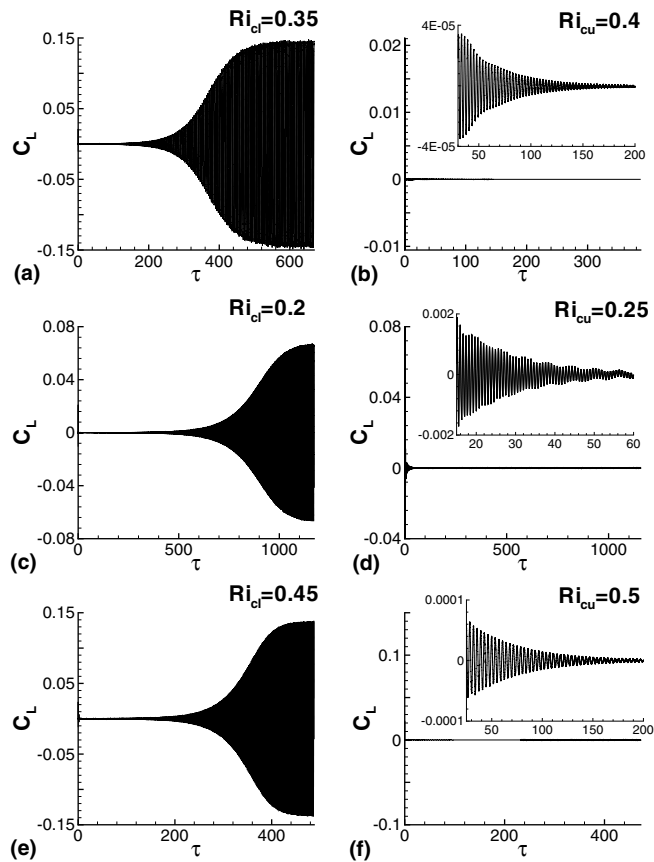

Fig. 8. Temporal variation of lift coefficient at the blockage ratio of (a,b) 10%; (c,d) 30% and (e,f) 50% for various critical Richardson number at $Re = 100$. In (b), (d) and (f), zoomed view is shown separately.

4.4. Breakdown of Kármán vortex street

The effect of channel-confinement of various degree at $Re = 100$ and increasing Re at $B/L = 30\%$ on the

breakdown of Kármán vortex street is shown in Fig. 10 with a stability envelope. The envelope has two boundaries, lower and upper as shown in the figure. The lower boundary corresponds to the observed Ri
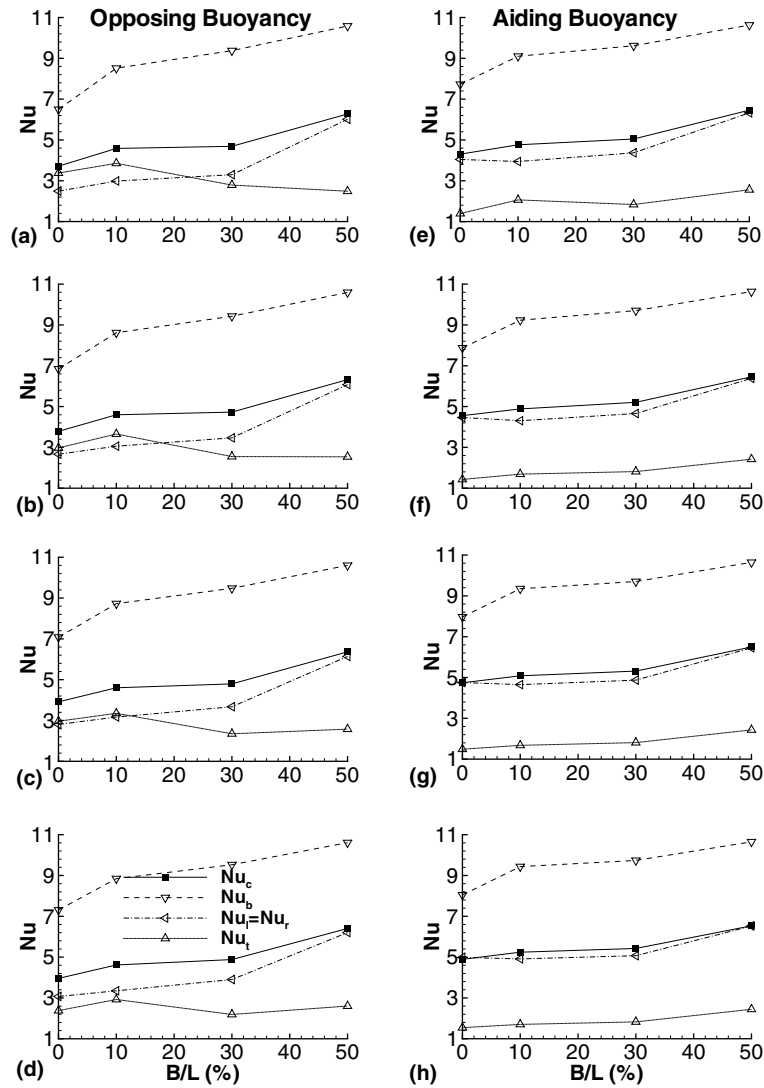
Fig. 9. Nusselt number (mean value for the periodic flow) for the cylinder and each of its faces as a function of blockage ratio for the Richardson number of (a) -1; (b) -0.75; (c) -0.5; (d) -0.25; (e) 0.25; (f) 0.5; (g) 0.75 and (h) 1, at $Re = 100$. Subscripts: b: bottom; t: top; l: left; r: right; c: cylinder average.

bound of the vortex-shedding flow and the upper one corresponds to the observed Ri bound for the breakdown of Kármán vortex street. These bounds, respectively, are the lower and upper value of critical Richardson number, Ri_{cl} and Ri_{cu}.

With increased heating, stability is imparted to the wake flow with a reduced entrainment of the far away fluid into the wake region. In our earlier work [5] for the forced-convective ($Ri = 0$) channel-confined flow, it was found that the critical Reynolds number for the onset of vortex shedding increases for $10\% \leqslant B/L \leqslant 30\%$ and decreases for $B/L \geqslant 40\%$. Thus, with increasing blockage ratio, the stability of the wake is enhanced by the channel-wall for $10\% \leqslant B/L \leqslant 30\%$ and reduced

for $B/L \geqslant 40\%$. Therefore, as the blockage ratio increases from 10% to 30% for a Reynolds number in the vortex shedding regime, say, it is reasonable to expect that less heating (Ri) is required to stabilize the flow to steady state due to increase in the channel induced stability, whereas, as the blockage ratio increases from 40% to 50%, more heating (Ri) should be needed due to decrease in the channel induced stability. Precisely this expected pattern is shown in Fig. 10(a) where a local minimum can be observed at $B/L = 30\%$. The increase in the stability of the flow when the blockage ratio increases from 10% to 30% is due to suppression of the propagation of disturbances causing wake instability by the channel wall [17]. Strykowski and Sreenivasan
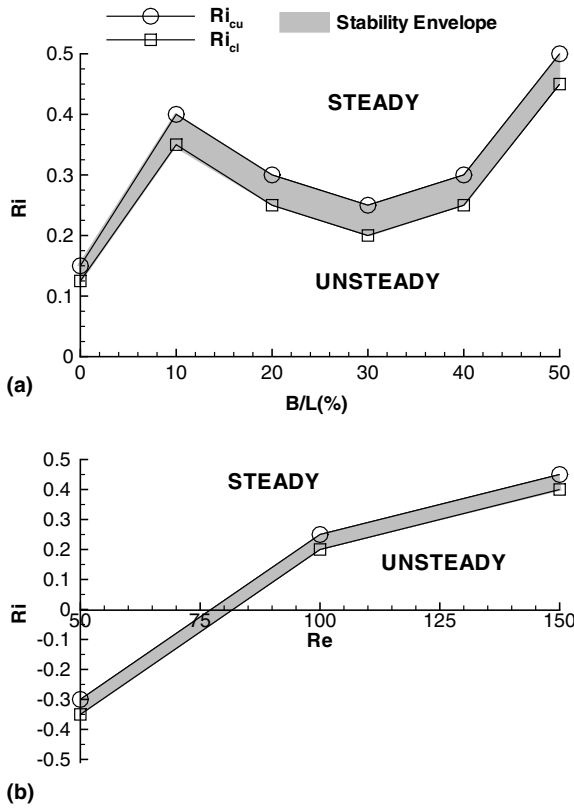
(a)

(b)

Fig. 10. Stability curve for the effect of (a) channel-confinement and (b) Reynolds number ($B/L = 30\%$) on breakdown of Kármán vortex street for the flow across a square cylinder at $Re = 100$. Note that Ri_{cl} is the lower and Ri_{cu} is the upper value of critical Richardson number for the breakdown of Kármán vortex street.

[18] suggested that at low Reynolds number, the vorticity pumped into the wake from the boundary layers on the cylinder can be diffused away from the shear layers merely by viscous action. The classical view is that as the flow Reynolds number increases viscous diffusion alone cannot keep up with the increased vorticity production in the upstream boundary layers, and vortices break away at regular intervals, constituting vortex shedding. Here, for $B/L \geqslant 40\%$, the cylinder wall shear layer also needs to diffuse the vorticity produced by the channel-wall in addition to that generated from the cylinder and thus, there is a decrease in the stability of the flow. The figure shows an increase in the critical Richardson number for the channel-confined flow at $B/L = 10\%$ as compared to the unconfined flow case. This is due to decrease in the stability of the wake for the confined flow case, which requires lower Re for the onset of vortex shedding at $Ri = 0$ [5] and here more heating (Ri) to weaken to the breakdown of Kármán vortex street at $Re = 100$. As mentioned in our earlier

work [7], better similarity is found here also between increasing Re at a constant Ri ($=0$ [5]) and increasing $1/Ri$ at a constant Re ($=100$, here).

The effect of varying Reynolds number on the breakdown of Kármán vortex street is shown in Fig. 10(b) for the channel-confined flow at $B/L = 30\%$. It shows that the critical Richardson number for the breakdown of Kármán vortex street increases with increasing Reynolds number at the constant blockage ratio. The figure also shows that vortex shedding can occur for the Reynolds number ($=50$), at which the flow is normally steady [5], when the cylinder is cooled with $Ri \leqslant -0.35$.
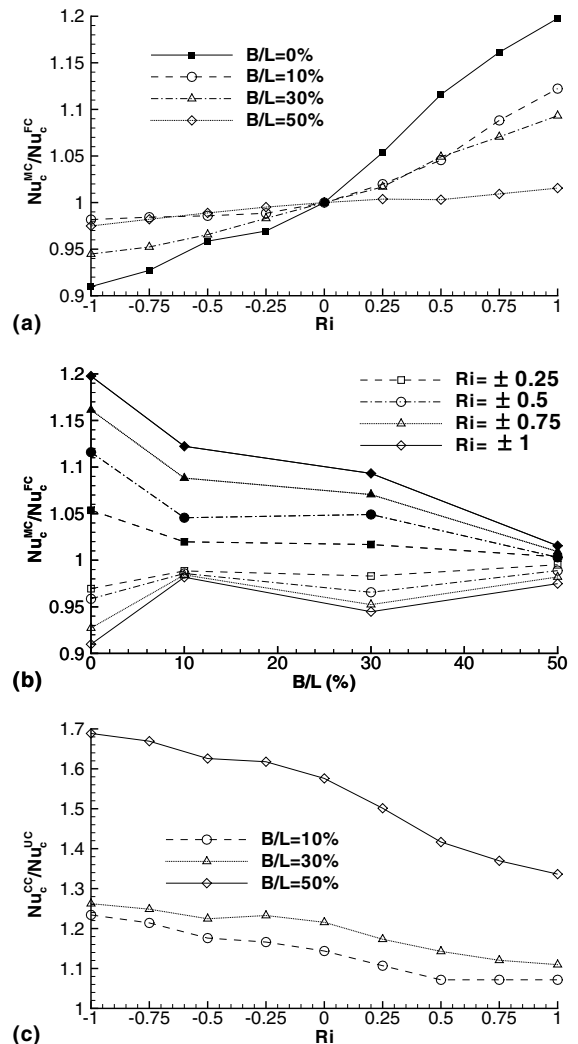

(a)

(b)

(c)

Fig. 11. Enhancement/suppression of heat transfer due to (a,b) aiding/opposing buoyancy; (c) channel-confinement as a function of (a,c) Richardson number and (b) blockage ratio. Note that the filled and unfilled symbols in (b) corresponds to the aiding and opposing buoyancy case, respectively.

4.5. Enhancement/suppression of heat transfer from the cylinder

Now, the attention is focussed on the enhancement/suppression of the average heat transfer from the cylinder caused by buoyancy and channel-confinement. To this end, the ratio of the average Nusselt number for the mixed convection (MC) case to that for the force convection (FC), Nu_c^{MC}/Nu_c^{FC}, and the ratio for the channel-confined (CC) flow to that for the unconfined (UC) flow, Nu_c^{CC}/Nu_c^{UC}, are plotted in Fig. 11 for various Richardson numbers and blockage ratios.

The effect of buoyancy on the heat transfer from the cylinder is a monotonic enhancement for the aiding ($Ri > 0$) and a monotonic suppression for the opposing buoyancy ($Ri < 0$) case, as shown in Fig. 11(a). However, the figure shows that the enhancement when the cylinder is heated is more than the suppression when it is cooled by the same temperature difference except for $B/L = 50\%$. With increasing blockage ratio, Fig. 11(b) show that the enhancement decreases monotonically with increasing blockage ratio at $Ri \geqslant 0.75$. For other Ri, the enhancement/suppression when compared to the unconfined flow decreases at $B/L = 10\%$, thereafter, it increases at $B/L = 30\%$ and decreases again at $B/L = 50\%$.

The effect of channel-confinement is an enhancement of heat transfer which decreases monotonically with increasing Ri and increases with increasing blockage ratio, shown in Fig. 11(c). The largest enhancement occurs for $B/L = 50\%$, which decreases from about 69% to less than 34% for the range of buoyancy parameter ($-1 \leqslant Ri \leqslant 1$) investigated.

5. Conclusions

The effect of channel-confinement on the vertical flow and heat transfer characteristics around a square cylinder maintained at a constant temperature has been studied, considering the effect of aiding and opposing buoyancy, between $-1 \leqslant Ri \leqslant 1$ for $B/L = 10\%$, 30% and 50% at $Re = 100$. At the constant Re, the minimum heating (critical Ri) required for the suppression of vortex shedding decreases with increasing blockage ratio up to a certain B/L ($=30\%$) value, but thereafter increases. At a constant blockage ratio ($=30\%$), the value of Ri at which vortex shedding degenerates increases with Re. At $Re = 50$ and $B/L = 30\%$—where there is normally steady twin vortices for the isothermal flow—the onset of vortex shedding is found after a certain minimum cooling of the cylinder. For the opposing buoyancy case at a constant Ri, both the width of the wake and entrainment of the fluid into the wake cavity decreases with increasing blockage ratio.

With increasing blockage ratio, a local maximum is found in the variation of mean recirculation length for $Ri \leqslant 0.25$ and a local minimum for the steady flow at $Ri \geqslant 0.5$, both at $B/L = 30\%$. The Strouhal number increases monotonically with increasing Ri and increasing blockage ratio. The pumping power increases with increasing blockage ratio at a constant Ri whereas with increasing Ri, it decreases monotonically for $B/L = 30\%$ and 50% and has a local minima for $B/H = 0\%$ and 10%. With increasing Ri, the minimum cylinder drag coefficient for the channel-confined flow occurs at the largest value of Ri for which vortex shedding is found. With increasing blockage ratio, the rms value of lift coefficient decreases monotonically for the opposing buoyancy whereas a local minimum is found at $B/L = 30\%$ for the aiding buoyancy ($Ri = 0$ and 0.25) case. The cylinder Nusselt number increases with increasing blockage ratio and increasing Ri. The heat transfer enhancement due to channel-confinement decreases with increasing Ri and increases with increasing blockage ratio.

References

[1] K. Suzuki, H. Suzuki, Unsteady heat transfer in a channel obstructed by an immersed body, in: C.L. Tien (Ed.), Annu. Rev. Heat Transfer, Begell House, New York, 1994, pp. 177–206.

[2] J.L. Rosales, A. Ortega, J.A.C. Humphrey, A numerical investigation of the convective heat transfer in unsteady laminar flow past a single and tandem pair of square cylinders in a channel, Numer. Heat Transfer A 38 (2000) 443–465.

[3] R.J. Yang, L.M. Fu, Thermal and flow analysis of a heated electronic component, Int. J. Heat Mass Transfer 44 (2001) 2261–2275.

[4] S. Turki, H. Abbassi, S.B. Nasrallah, Two-dimensional laminar fluid flow and heat transfer in a channel with a built-in square cylinder, Int. J. Them. Sci. 42 (2003) 1105–1113.

[5] A. Sharma, V. Eswaran, Effect of channel confinement on the two-dimensional laminar flow and heat transfer across a square cylinder, Numer. Heat Transfer A 46 (2004) 1–29.

[6] K.S. Chang, J.Y. Sa, The effect of vortex shedding in the near wake of a circular cylinder, J. Fluid Mech. 220 (1990) 253–266.

[7] A. Sharma, V. Eswaran, Effect of aiding and opposing buoyancy on the heat and fluid flow across a square cylinder at $Re = 100$, Numer. Heat Transfer A 45 (2004) 601–624.

[8] B. Farouk, S.I. Güceri, Natural and mixed convection heat transfer around a horizontal cylinder within confining walls, Numer. Heat Transfer 5 (1982) 329–341.

[9] C.J. Ho, M.S. Wu, J.B. Jou, Analysis of buoyancy-aided convection heat transfer from a horizontal cylinder in a vertical duct at low Reynolds Number, Wärme-und Stoffübertragung 25 (1990) 337–343.

[10] K. Nakabe, H. Hasegawa, K. Matsubara, K. Suzuki, Heat Transfer from a heated cylinder in a flow between parallel

plates in a free-forced combined convection regime, in: Proc. 9th Int. Symp. on Transport Phenomena in Thermal Fluids Engg., Singapore, 1996, pp. 651–656.

[11] S. Singh, G. Biswas, A. Mukhopadhyay, Effect of thermal buoyancy on the flow through a vertical channel with a built-in circular cylinder, Numer. Heat Transfer A 34 (1998) 769–789.

[12] G. Biswas, H. Laschefski, N.K. Mitra, M. Fiebig, Numerical investigation of mixed convection heat transfer in a horizontal channel with a built-in square cylinder, Numer. Heat Transfer A 18 (1990) 173–188.

[13] A. Sharma, V. Eswaran, Heat and fluid flow across a square cylinder in the two-dimensional laminar flow regime, Numer. Heat Transfer A 45 (2004) 247–269.

[14] A. Sharma, Numerical investigation of unconfined and channel-confined flow across a square cylinder with forced and mixed convection heat transfer, PhD Thesis, Indian Institute of Technology Kanpur, India, 2003.

[15] V. Eswaran, S. Prakash, A finite volume method for Navier–Stokes equations, in: Proc. Third Asian CFD Conf., Bangalore, India, 1998, pp. 127–136.

[16] A. Sharma, V. Eswaran, A finite volume method, in: K. Muralidhar, T. Sundararajan (Eds.), Computational Fluid Flow and Heat Transfer, Narosa Publishing House, New Delhi, 2003, pp. 445–482.

[17] F.H. Shair, A.S. Grove, E.E. Pertersen, A. Acrivos, The effect of confining walls on the stability of the steady wake behind a circular cylinder, J. Fluid Mech. 17 (1963) 547–550.

[18] P.J. Strykowski, K.R. Sreenivasan, On the formation and suppression of vortex shedding at low Reynolds Numbers, J. Fluid Mech. 218 (1990) 71–107.